Accepted Manuscript

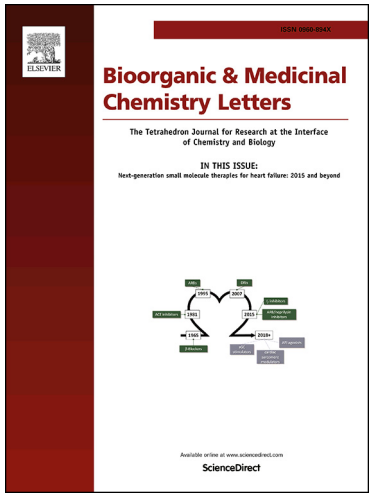

The Discovery of Novel 3-Aryl-Indazole Derivatives as Peripherally Restricted Pan-Trk Inhibitors for the Treatment of Pain

Hiromitsu Shirahashi, Eisuke Toriihara, Yoshihito Suenaga, Hideyuki Yoshida, Kensuke Akaogi, Yukiko Endou, Makoto Wakabayashi, Misato Takashima

PII: S0960-894X(19)30398-1
DOI: https://doi.org/10.1016/j.bmcl.2019.06.018
Reference: BMCL 26496

To appear in: *Bioorganic & Medicinal Chemistry Letters*

Received Date: 4 April 2019
Revised Date: 24 May 2019
Accepted Date: 15 June 2019

Please cite this article as: Shirahashi, H., Toriihara, E., Suenaga, Y., Yoshida, H., Akaogi, K., Endou, Y., Wakabayashi, M., Takashima, M., The Discovery of Novel 3-Aryl-Indazole Derivatives as Peripherally Restricted Pan-Trk Inhibitors for the Treatment of Pain, *Bioorganic & Medicinal Chemistry Letters* (2019), doi: https://doi.org/10.1016/j.bmcl.2019.06.018

The Discovery of Novel 3-Aryl-Indazole Derivatives as Peripherally Restricted Pan-Trk Inhibitors for the Treatment of Pain

Hiromitsu Shirahashi*, Eisuke Toriihara, Yoshihito Suenaga, Hideyuki Yoshida, Kensuke Akaogi, Yukiko Endou, Makoto Wakabayashi, Misato Takashima*

Pharmaceuticals Research Center, Asahi Kasei Pharma Corporation, 632-1 Mifuku, Izunokuni, Shizuoka 410-2321, Japan

*Correspondence:
Hiromitsu Shirahashi, E-mail address: shirahashi.hd@om.asahi-kasei.co.jp
Misato Takashima, E-mail address: takashima.mc@om.asahi-kasei.co.jp

Abstract
The design, synthesis, and biological evaluation of novel 3-aryl-indazole derivatives as peripherally selective pan-Trk inhibitors are described. Three strategies were used to obtain a potent compound exhibiting low central nervous system (CNS) penetration and high plasma exposure: 1) a structure-based drug design (SBDD) approach was used to improve potency; 2) a substrate for an efflux transporter for lowering brain penetration was explored; and 3) the most basic pKa (pKa–MB) value was used as an indicator to identify compounds with good membrane permeability. This enabled the identification of the peripherally targeted **17c** with the potency, kinase-selectivity, and plasma exposure required to demonstrate in vivo efficacy in a Complete Freund's adjuvant (CFA)-induced thermal hypersensitivity model.

Keywords: pan-Trk inhibitor; peripherally restricted; 3-aryl-indazole derivative; efflux transporter; pKa-MB

Tropomyosin-related kinase (Trk) is a family of receptor tyrosine kinases highly expressed in neurons, comprised of three isomers TrkA, TrkB, and TrkC. Each isomer is activated by the binding of a complementary neutrophin, such as nerve growth factor (NGF) for TrkA, brain-derived neurotrophic factor (BDNF) for TrkB, and neurotrophin-3 for TrkC.[1] The activation of Trk causes dimerization and autophosphorylation, followed by initiation of the intracellular signaling pathway.[1,2] Trk signaling pathways are implicated in various cancers and pain.[3,4,5] We have a particular interest in the NGF/TrkA signaling pathway because preclinical studies on antagonists of NGF and clinical research on a humanized anti-NGF monoclonal antibody (tanezumab) suggest that NGF plays a crucial role in pain.[6,7,8]

Trk inhibitors can cause CNS side effects. The inhibition of NGF/TrkA signaling in the CNS may induce dysfunction in the cholinergic circuitry[9] and BDNF/TrkB signaling in the CNS appears to regulate hippocampal long-term potentiation and eating behavior.[10,11] The highly homologous nature of the ATP binding sites in TrkA, B and C severely hampers the design of small molecules with high selectivity towards Trk family members.[12] We considered the CNS-related risk and high similarity of the ATP binding sites of the Trk family proteins and explored a peripherally selective small molecule as a pan-Trk inhibitor for the treatment of chronic pain.

We embarked on the design and synthesis of a substrate for efflux transporters to obtain a safe orally administrable compound with restricted CNS penetration. Whether a compound is an efflux transporter substrate or not can be assessed by the efflux ratio (ER) value obtained by in vitro assays. In our Trk inhibitor program, the Caco-2 assay was used to calculate ER values. Compounds having ER values over 2 were evaluated as efflux transporter substrates.[13]

Screening of our in-house compound library identified hit **1** exhibiting moderate potency (Figure 1). We therefore optimized hit **1** by focusing on the A part (substituted pyridine moiety) and the B part (substituted benzylamine moiety), while maintaining the 3-aryl-indazole structure as our original hinge binder. This structure is not found in known pan-Trk inhibitors such as **2** (AZ-23) and **4** (Figure 2).[14a,15,16] While compound **3** (Entrectinib) has an indazole structure, the nitrogen atom at the 3-position is important for binding with the hinge.

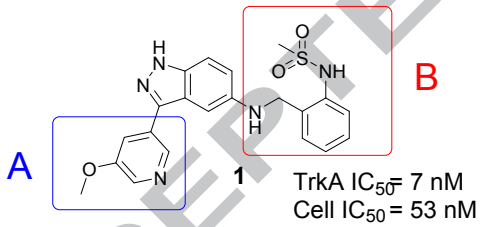

Figure 1. The structure of hit **1**.

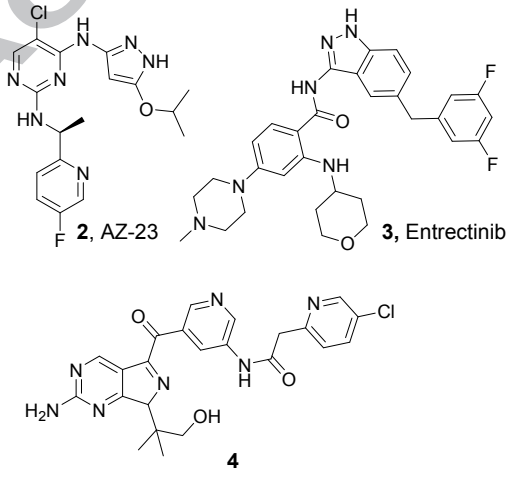

Figure 2. Trk inhibitors described in the literature.

First, we optimized the A part with the aim of improving the potency and metabolic stability. The structure activity relationship (SAR) of the A part is summarized in Table 1. Potency and metabolic stability appeared to be affected by the position of the nitrogen atom and the orientation of the substituent group in the pyridine moiety (**1**, **10a** and **10b**). Regarding the methoxypyridine derivatives, **10b** exhibited the highest potency and moderate metabolic stability. Substitution of the methoxy group in **10b** by 4-hydroxypiperidine or 4-aminopiperidine maintained the potency in an enzyme assay and metabolic stability but decreased the potency in a cell-based assay (**10c** and **10d**). These results suggested that the larger substituents were tolerated at R^1 and that the low membrane permeability of these compounds probably decreased their potency in the cell-based assay (the Madine−Darby canine kidney cell (MDCK) apparent permeability coefficients (P_{app}) at pH 7.4 of **10c** and **10d** were both 0.3×10^{-6} cm/sec). Indeed, **10e** possessing a larger substituent than methoxy group at R^1, which has a higher membrane permeability (MDCK P_{app} at pH 7.4 of 1.2×10^{-6} cm/sec) than **10c** or **10d**, showed excellent potency in both the enzyme and cell-based assays as well as good metabolic stability.

The binding mode of **10e** was confirmed via X-ray crystallography using a 2.3 Å complex structure with TrkA protein (Figure 3). Compound **10e** was found to be a Type I inhibitor that binds to the DFG-in conformation of TrkA. Figure 3 shows that the indazole ring of **10e** interacts with the kinase hinge through two key hydrogen bonds between Glu590 and Met592, and that the piperazine and benzylamine moieties (in the B part) do not appear to form hydrogen bonds with TrkA. The observation that the piperazine group is located at the entrance to solvent region, is considered to be the reason why the substituent larger than methoxy group was allowed at R^1.

As mentioned above, **10e** exhibited high potency, good metabolic stability, and high ER value (Caco-2 ER = 7.8), and the interaction with TrkA, However, we considered that the membrane permeability of **10e** was still not high enough to be administered orally. We therefore conducted further SAR development of the B part in **10e** to improve the permeability.

Table 1. SAR of the A part of hit **1**

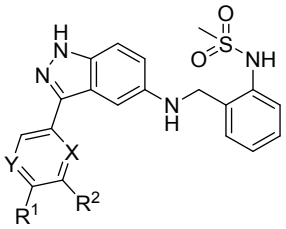

ID	R^1	R^2	X	Y	TrkA IC_{50} (nM)	Cell IC_{50} (nM)	hCLint[a] (mL/min/kg)

1	H	-OMe	C	N	7.0	53	217
10a	H	-OMe	N	C	7.8	64	833
10b	-OMe	H	C	N	2.9	35	359
10c	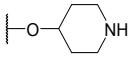	H	C	N	2.3	175	323
10d	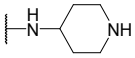	H	C	N	0.9	224	184
10e	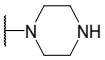	H	C	N	1.6	27	70

[a]hCLint was determined from human liver microsome incubations; ND = not determined.

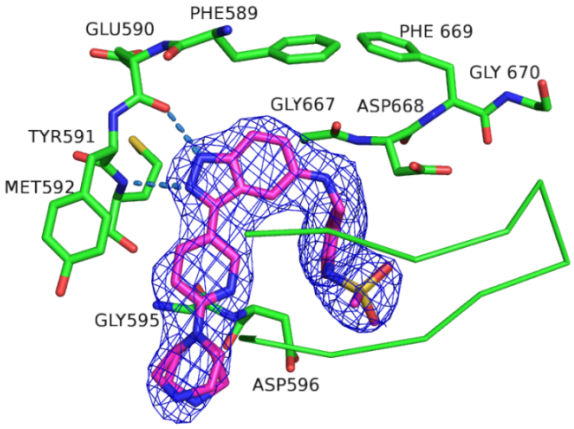

Figure 3. Co-crystal structure of **10e** bound to TrkA protein in a DFG-in conformation. Two key hydrogen bonds are highlighted with blue dashed lines. Nitrogen atoms are shown in blue, oxygen atoms in red, and the sulfur atom in yellow. Some protein residues were omitted for clarity. The PDB code for **10e** is 6J5L.

We first studied the SAR of the linker structure using a compound with a simple phenyl group to facilitate synthesis of the derivatives (Table 2). The results suggested that a non-branched nitrogen linker is the most suitable structure in terms of potency, metabolic stability and membrane permeability (**13c, 22a, 22b, 22c** and **22d**). The potency reduction of **22c** and **22d** indicated that the space around the linker was not enough to introduce a substituent. The decreased metabolic stability of **22a** and **22d** was considered to be due to the increased lipophilicity. Compound **22a** has two benzyl positions that might be metabolized.

Next, we explored the SAR of substituents on the phenyl group (Table 3) and found that the 2-substituted derivative was more potent than the 3-or 4-substituted derivatives (**10e, 13a** and **13b**). Furthermore, replacement of the methanesulfonamide group with the methanesulfonyl group improved potency in the cell-based assay and retained potency in the enzyme assay (**13d**). In addition, **13d** exhibited higher membrane permeability and ER than **10e** while maintaining metabolic stability**.** The improvement of membrane permeability might be achieved by the decrease of the hydrogen bond donors (HBD). The increase of the ER value implied that the methanesulfonyl group had a higher affinity for the efflux transporter than the methanesulfonamide group.

Figure 4 shows an overlay of **10e** and AZ-23 bound to TrkA protein in which the *para*-position of the methanesulfonyl group in **10e** corresponds to the space occupied by the fluorine atom in the fluoropyridine ring of AZ-23. The fluorine atom in AZ-23 was reported to contact the backbone carbonyl atom of Asn 665 and the Cα of Gly 667 N-terminal to the DFG sequence of the activation loop,[14a] and to be important for the high potency against TrkA.[14b] Thus, we predicted that the introduction of a fluorine atom at the *para*-position of the methanesulfonyl group in **13d** could improve the potency, and as expected, the *para*-fluorinated analogue **13e** exhibited higher potency than **13d**. In addition, the fluorine substitution improved the ER value but decreased the membrane permeability. The reason for the increase of ER value can be considered that the efflux transporter affinity was enhanced by introducing fluorine atom. On the other hand, there is the report that the increase in molecular weight due to the insertion of fluorine does not lead to increased ER value, although high molecular weight tends to show high ER value.[17] Therefore, the cause of the increase of ER value with the fluorine introduction was considered to be increase of molecular weight, which may be exceptionally cased only in our compounds.

Table 2. SAR of the linker structure of the B part of **10e**

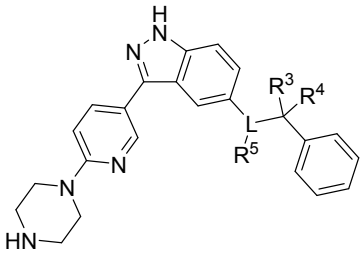

ID	L	R^3	R^4	R^5	TrkA IC_{50} (nM)	Cell IC_{50} (nM)	hCLint[a] (mL/min/kg)	MDCK P_{app}[b] (cm/sec)
13c	N	H	H	H	12.3	73	12	13.0×10^{-6}
22a	CH	H	H	H	18.1	>300	2726	3.1×10^{-6}
22b	O	H	H	-	11.1	127	694	9.6×10^{-6}
22c	N	H	H	Me	27.6	264	417	7.3×10^{-6}

22d	N	Me	Me	H	58.6	253	1737	11.0×10^{-6}

[a]hCLint was determined from human liver microsome incubations; [b]MDCK P_{app} was evaluated at pH 7.4.

Table 3. SAR of the substituted phenyl ring of the B part of **10e**

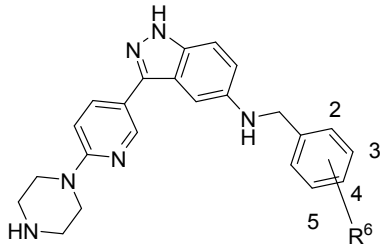

ID	R^6	TrkA IC_{50} (nM)	Cell IC_{50} (nM)	hCLint[a] (mL/min/kg)	MDCK P_{app}[b] (cm/sec)	Caco-2 ER
10e	2-NH-SO_2Me	1.6	27	69.5	1.2×10^{-6}	7.8
13a	3-NH-SO_2Me	143.2	ND	ND	ND	ND
13b	4-NH-SO_2Me	766.2	ND	ND	ND	ND
13d	2-SO_2Me	1.4	16	74	12.5×10^{-6}	13.6
13e	2-SO_2Me-5-F	0.3	2	176	0.4×10^{-6}	71.1

[a]hCLint was determined from human liver microsome incubations; [b]MDCK P_{app} was evaluated at pH 7.4; ND = not determined.

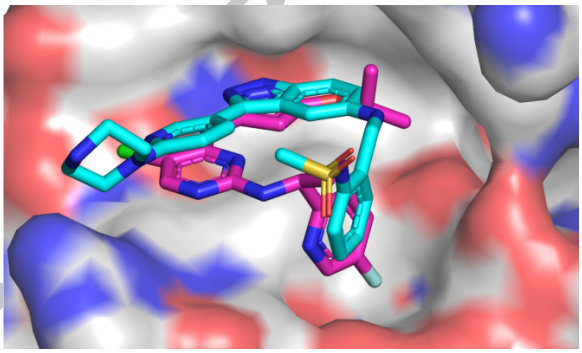

Figure 4. Overlay of **10e** and AZ-23 bound to TrkA protein. The PDB code for **AZ-23** is 4AOJ.[14a]

The in vivo PK profiles of **13d** and **13e** were determined but the concentration of these compounds in plasma was below the detection limit when administered orally at a dose of 10 mg/kg to SD rats. Thus, we investigated the underlying cause of the poor plasma exposure of these compounds (Table 4). Although **13d** showed good membrane permeability at pH 7.4 (Table 3), we considered that the membrane permeability was the reason for their poor plasma exposure, because both **13d** and **13e**

had the piperazine group that is likely ionizable in the small intestine, and the membrane permeability of ionized compounds is typically lower than that of non-ionized compounds. We therefore confirmed whether **13d** and **13e** would be ionized in the small intestine by calculating the most basic pKa (pKa-MB) of these compounds with ACD/Percepta, since pKa determines the degree of ionization. As a result, more than 99% of both **13d** and **13e** was estimated to be ionized at pH 6.5, the pH of the small intestine,[18] and the terminal amino group in the piperazine moiety was found to be the most basic site in these compounds. Moreover, the membrane permeability of **13d** at pH 6.5 dramatically decreased from the membrane permeability at pH 7.4, possibly due to increased ionization of the compound. This result indicated that the membrane permeability at pH 6.5 was important to impart good plasma exposure to a compound. These findings suggest that the membrane permeability of **13d** and **13e** at pH 6.5 might be too low, resulting in poor plasma exposure and the piperazine group might cause low membrane permeability.

Table 4. pKa-MB value, ionized portion, and membrane permeability of **13e** at pH 6.5

ID	pKa-MB	Ionized portion at pH 7.4[a]	Ionized portion at pH 6.5[a]	MDCK P_{app} at pH 7.4 (cm/sec)	MDCK P_{app} at pH 6.5 (cm/sec)
13d	8.55	73.7 %	> 99.1%	12.5×10^{-6}	0.4×10^{-6}
13e	8.55	73.7 %	> 99.1%	0.4×10^{-6}	0.3×10^{-6}

[a]Ionized portion was determined from the Henderson-Hasselbach equation; [b]MDCK P_{app} was evaluated at both pH 6.5 and pH 7.4.

Consequently, we identified an alternative structure to the piperazine group by conducting another SAR exploration of the A part of **13e** while retaining the structure of the B part (predicted to contribute to high potency) (Table 5). The pKa-MB and membrane permeability at pH 6.5 were also examined as indices for compound selection for an in vivo pharmacokinetics (PK) study.

The results shown in Table 5 suggested that removal of the piperazine group would yield the desired pKa-MB values and increase the membrane permeability significantly at pH 6.5. Unfortunately, the pyridine derivatives **17a** and **17b** exhibited decreased metabolic stability; however, the pyrazole derivatives **17c** and **13f** showed metabolic stability comparable to **13e**. **17c** exhibited the same potency as **13e**, providing a possible substrate for an efflux transporter (Caco-2 ER = 12.6), and exhibited the best balance of potency, metabolic stability, and membrane permeability of the compounds synthesized. We determined the in vivo PK characteristics of **17c** by administering it orally at a dose of 5 mg/kg to SD rats and found that the C_{max} of **17c** was moderate (161.0 nmol/L) and there was very low CNS penetration (brain/plasma concentration ratio (B/P) = 0.03) (Table 6).

Table 5. SAR of the A part of **13e**

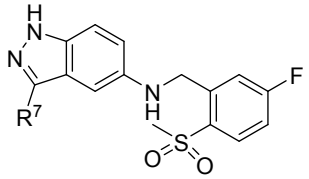

ID	R^7	TrkA IC_{50} (nM)	Cell IC_{50} (nM)	hCLint[a] (mL/min/kg)	MDCK P_{app} (cm/sec)[b]	Solubility (μM)	pKa-MB[c]	Caco-2 ER
13e	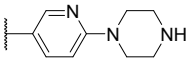	0.3	2.0	177.5	0.3×10^{-6}	38.7	8.5	71.1
17a		0.2	2.4	793.4	61.5×10^{-6}	23.0	4.8	ND
17b		2.1	18.0	442.7	73.2×10^{-6}	15.2	3.9	ND
17c	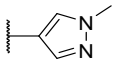	0.2	1.7	127.4	15.2×10^{-6}	140.7	2.6	12.6
13f	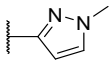	4.5	104.8	136.8	34.0×10^{-6}	80.1	2.3	ND

[a]CLint determined from human liver microsome incubations; [b] MDCK P_{app} was evaluated at pH 6.5; [c]pKa-MB determined by ACD calculation; ND = not determined.

Table 6. Summary of the PK properties of **17c**

C_{max} (nmol/L)[a]	161.0
CL (L/h/kg)[b]	4.4
$T_{1/2}$ (h)[c]	1.46
plasma protein binding (%)	86.6
brain protein binding (%)	96.2
B/P[d]	0.03

[a]C_{max} was determined by the oral dosing of SD rats at 5 mg/kg; [b]CL and [c]$T_{1/2}$ were determined by intravenous administration to SD rats at 1 mg/kg; [d]B/P was determined by intraperitoneal administration to SD rats at 2.5 mg/kg.

We investigated the kinase selectivity of **17c** at 20 nM against a panel of 49 kinases and found that no kinase was inhibited by more than 50%, excluding TrkA, and this compound exhibited no selectivity against TrkB (TrkB IC_{50} = 0.2 nM). The selectivity of **17c** against TrkC was not determined. We concluded that **17c** had sufficient selectivity as a pan-Trk inhibitor to warrant evaluating its in vivo efficacy.

We investigated the effect of **17c** in an inflammatory pain model using a CFA-induced thermal hypersensitivity assay. Compound **17c** was orally administered to rats at increasing doses once daily after administration of CFA. Table 7 shows the plasma and brain levels of **17c** at 1 h post-dose. The concentration of **17c** in the brain was too low to detect at doses of 0.8 mg/kg and 4.0 mg/kg. Correction for plasma protein binding revealed that even at a dose of 0.8 mg/kg, there was a higher concentration of unbound **17c** in plasma than the IC_{50} value obtained by the cell-based assay. Figure 5 shows the rate of weight gain of rats to which **17c** was administered. The weight gain was established as 100 mg/kg. This is considered to be caused by the inhibition of BDNF/TrkB signaling in the CNS by increased brain penetration of **17c**.[11] Therefore, as a peripherally selective pan-Trk inhibitor, the acceptable dosing amount could be up to 20 mpk because no weight gain was observed. Figure 6 demonstrates the results of the CFA-induced thermal hypersensitivity assay using **17c**. A dose of 0.8 mg/kg seemed to provide weak efficacy and doses of 4.0, 20, and 100 mg/kg had a tendency for reversed thermal hyperalgesia comparable to a dose of 100 mg/kg ibuprofen. Although no dose dependency was observed, we considered the reason the maximum effect was achieved at 4.0 mg/kg (p-value was 0.0522) was because there was an individual difference in rats (p-values were 0.2531 at 20 mg/kg and 0.2875 at 100 mg/kg).

Table 7. Plasma and brain concentrations of **17c** 1 h post-dose

Dose (mg/kg)	$C_{u,plasma}$[a] (nM)	$C_{u,plasma}/IC_{50}$	$C_{u,brain}$[b] (nM)	$C_{u,brain}/IC_{50}$
0.8	4.7	2.8	BLQ[c]	-
4.0	14.9	8.8	BLQ[c]	-
20.0	70.9	41.7	1.5	0.9
100.0	266.5	156.8	3.5	2.1

[a]$C_{u,plasma}$ and [b]$C_{u,brain}$ were determined by oral administration to CFA rats; [c]BLQ means "below limit of quantification."

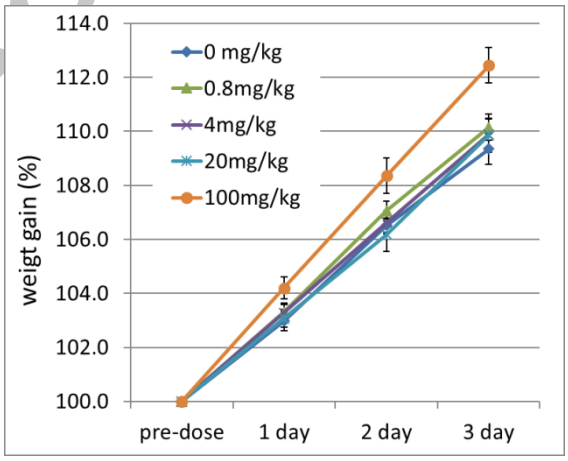

Figure 5. Weight gain rate of rat to which **17c** was administered

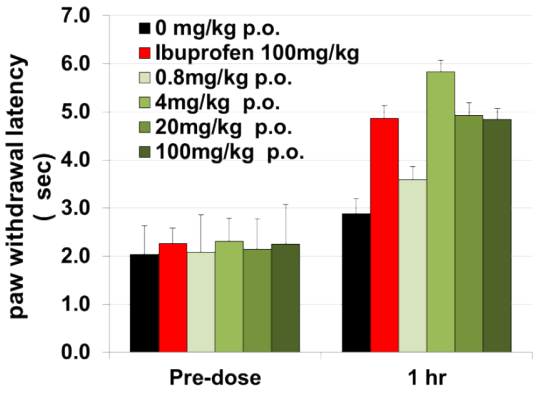

Figure 6. Results of CFA-induced thermal hypersensitivity assay using **17c.**

The indazole derivatives listed in Tables 1, 2, 3 and 5 were synthesized as outlined in Schemes 1 and 2. Scheme 1 starts with the hydrogenation of **5** to form **6**, followed by reductive amination to afford **7** and **14**. Suzuki-Miyaura coupling of **7** with the corresponding boronic acid or pinacol boronate gave **8a-b**. **9a-e** were prepared via a nucleophilic aromatic substitution reaction in which **8a-b** were reacted with the corresponding alcohol or amine. Deprotection of the THP group in **9a-e** provided **10a-e**. **14** was reacted with an organotin reagent to obtain **15**, which was converted into **16a-c** by Stille coupling. The deprotection of **16a-c** furnished **17a-c**. **6** was reacted with the corresponding pinacol boronate to form **11a-b**. The reductive amination of **11a-b** with the corresponding aldehyde afforded **12a-f**, which were converted to **13a-f** by deprotection of the THP group. The synthetic route to **22a-d** is shown in Scheme 2. Commercially available **18** was protected using the THP group to obtain **19**, which was converted to **20** by Suzuki-Miyaura coupling. A second Suzuki-Miyaura coupling and Buchwald–Hartwig aryl amination of **20** provided **21a** and **21b-c**, respectively. **21d** was prepared by reaction with benzyl bromide and **24**, which was synthesized from commercially available **23** by Suzuki-Miyaura coupling. The hydrogenation of **21a** afforded **21e** and deprotection of **21b-e** provided **22a-d**.

In conclusion, we identified the novel 3-aryl-indazole derivative **17c** as a low-CNS-penetrating targeted small molecule pan-Trk inhibitor. Three methodologies contributed to the design of this compound: 1) employing the SBDD approach; 2) exploring a substrate as an efflux transporter; and 3) calculating the value of pKa–MB. Compound **17c** exhibited sub-nanomolar potency, high selectivity, and satisfactorily low brain penetration, and in addition demonstrated dose-independent in vivo efficacy in a CFA-induced thermal hypersensitivity model.

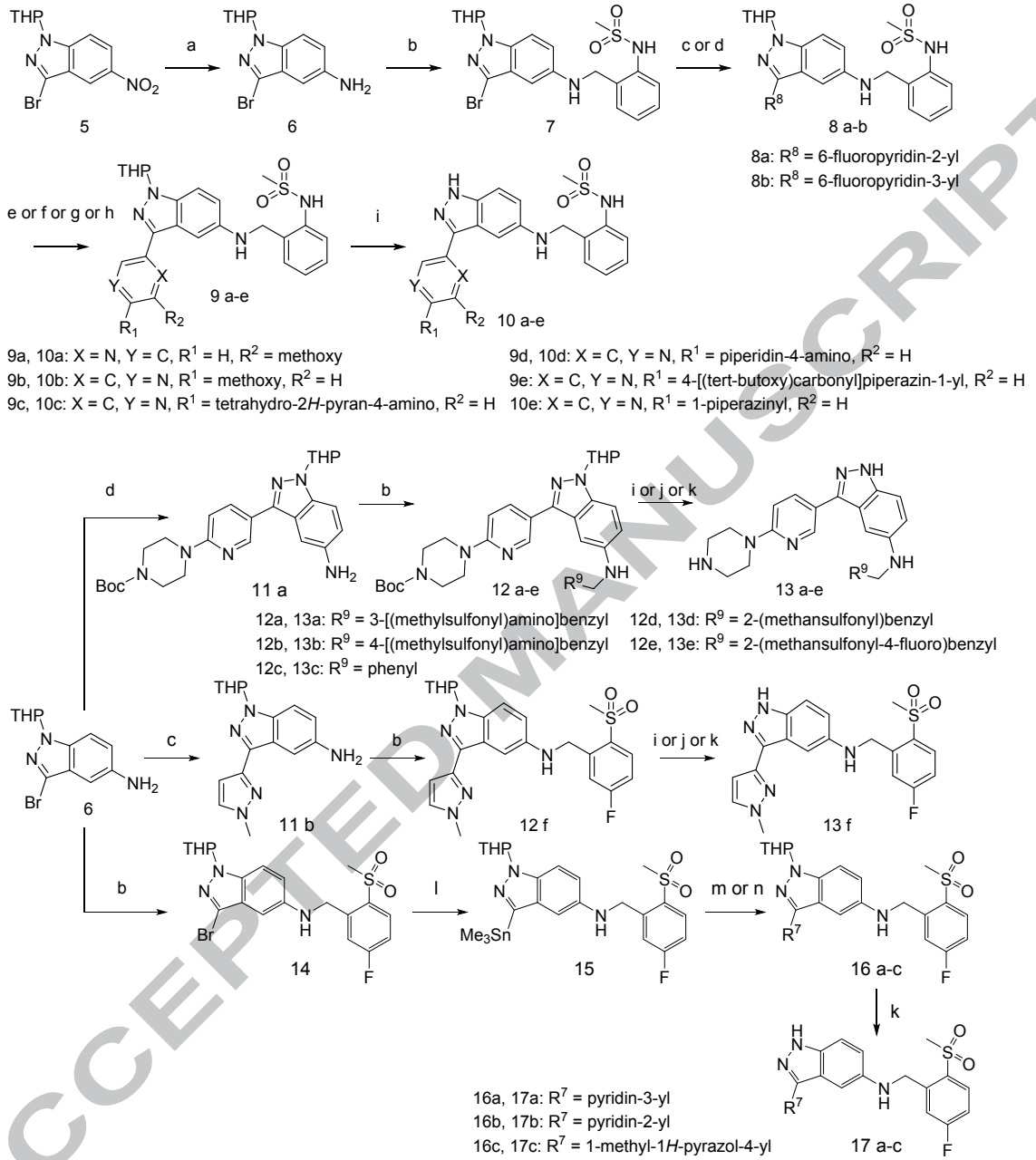

Scheme 1. Synthesis of **10a-e**, **13a-f** and **17a–c**. Reagents and conditions: (a) H_2 gas, Pt(S)/C, THF, 30 °C, 70%; (b) corresponding aldehyde, $NaBH_3CN$, AcOH, MeOH-THF, rt; (c) corresponding pinacol boronate, $PdCl_2(dppf)\cdot CH_2Cl_2$, 2 M Na_2CO_3 in H_2O, DME, 90 °C or 95 °C, 39%-quant; (d) corresponding boronic acid or pinacol boronate, $Pd(PPh_3)_4$, Na_2CO_3 or K_2CO_3, DME-H_2O, 80 °C or 85 °C, 64-74%; (e) NaOMe, MeOH, 60 °C; (f) 1-(tert-butoxycarbonyl)-4-hydroxypiperidine, tBuOK, DMSO, rt; (g) 1-(tert-butoxycarbonyl)-4-aminopiperidine, DMSO, 80 °C to 100 °C; (h)1-(tert-butylcarbonyl)piperazine, DMSO, 80 °C; (i) TFA, CH_2Cl_2, rt, 9-63% (two steps); (j) 2 M HCl in MeOH, rt, 17-70% (two steps); (k) 4 M HCl in 1,4-dioxane, 1,4-dioxane, rt, 2-23% (two steps); (l)

hexamethylditin, $Pd(PPh_3)_4$, 1,4-dioxane, 80 °C, 38%; (m) corresponding bromide, $Pd(PPh_3)_4$, LiCl, DMF, 60 °C; (n) 4-bromo-1-methylpyrazole, $Pd(PPh_3)_4$, DMF, 90 °C;

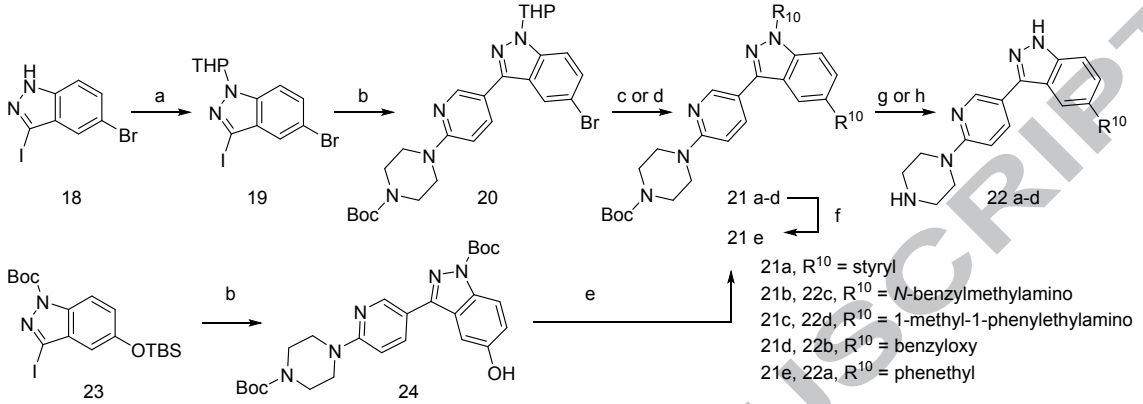

Scheme 2. Synthesis of **22a-d**. Reagents and conditions: (a) DHP, TsOH-H_2O, toluene, 60 °C, 89%; (b) 2-(4-tert-Butoxycarbonylpiperazin-1-yl)pyridine-5-boronic acid, pinacol ester, $Pd(PPh_3)_4$, K_2CO_3, DME-H_2O, 80 °C, 68%-quant; (c) *trans*-2-phenylvinylboronic acid, $Pd(PPh_3)_4$, K_2CO_3, DME-H_2O, 100 °C; (d) corresponding benzylamine, Pd(crotyl)Q-PhosCl, tBuONa, toluene, 35 °C or 100 °C; (e) benzyl bromide, K_2CO_3, acetone, rt, 61% (two steps); (f) H_2 gas, Pd/C, MeOH-EtOAc, rt, 89% (two steps); (g) TFA, CH_2Cl_2, rt, 51%; (h) 4 M HCl in 1,4-dioxane, rt, 44-51%.

Abbreviations

ATP, adenosine triphosphate; BDNF, brain-derived neurotrophic factor; B/P, brain/plasma concentration ratio; CFA, Complete Freund's adjuvant; CL, clearance; $T_{1/2}$, half-life; CLint, intrinsic clearance; CNS, central nervous system; $C_{u,brain}$, unbound brain concentration; $C_{u,plasma}$, unbound plasma concentration; ER, efflux ratio; HBD, hydrogen bond donor; IC_{50}, half-maximum inhibitory concentration; MDCK, Madine−Darby canine kidney; ND, not determined; NGF, nerve growth factor; Papp, apparent permeability; PDB, Protein Data Bank; PK, pharmacokinetics; pKa–MB, most basic pKa; SBDD, structure based drug design; Trk, tropomyosin-related kinase

Acknowledgments

We are grateful to Shinichi Oguma, Tsuyoshi Arai and Naomi Shinotsuka for conducting the biological evaluations, and to Tokuhito Goto and Tomohisa Toyama for their insightful chemistry support.

Notes

The authors declare no competing financial interest.

REFERENCES

(1) Nemat Khan, Maree T. Smith. Neurotrophins and Neuropathic Pain: Role in Pathobiology. *Molecules.* 2015;20:10657−10688.

(2) David R Kaplan, Freda D Miller. Neurotrophin signal transduction in the nervous system. *Curr. Opin. Neurobiol.* 2000;10:381−391.

(3) Patrick W. Mantyh, Martin Koltzenburg, Lorne M. Mendell, Leslie Tive, *et al*. Antagonism of Nerve Growth Factor-TrkA Signaling and the Relief of Pain. *Anesthesiology.* 2011;115:189−204.

(4) Akira Nakagawara. Trk receptor tyrosine kinases: a bridge between cancer and neural development. *Cancer Lett*. 2001;169:107−114.

(5) Marco A. Pierotti, Angela Greco. Oncogenic rearrangements of the NTRK1/NGF receptor. *Cancer Lett*. 2006;232:90−98.

(6) Franz F. Hefti, Arnon Rosenthal, Patricia A. Walicke, *et al*. Novel class of pain drugs based on antagonism of NGF. *Trends Pharmacol. Sci.* 2006;27:85−91.

(7) Nancy E. Lane, Thomas J. Schnitzer, Charles A. Birbara, *et al*. Tanezumab for the treatment of pain from osteoarthritis of the knee. *N. Engl. J. Med.* 2010;363:1521−1531.

(8) T.J. Schnitzer, N.E. Lane, C. Birbara, *et al*. Long-term open-label study of tanezumab for moderate to severe osteoarthritic knee pain. *Osteoarthr. Cartil.* 2011;9:639−646.

(9) Efrain Sanchez-Ortiz, Daishi Yui, Dongli Song, *et al*. TrkA gene ablation in basal forebrain results in dysfunction of the cholinergic circuitry. *J. Neurosci.* 2012;32:4065−4079.

(10) Liliana Minichiello. TrkB signalling pathways in LTP and learning. *Nat. Rev. Neurosci.* 2009;10:850−860.

(11) Brittany L. Mason, Mary Kay Lobo, Luis F. Parada, *et al*. Trk B signaling in dopamine 1 receptor neurons regulates food intake and body weight. *Obes.* 2013;21:372−2376

(12) T. Bertrand, M. Kothe, J. Liu, *et al*. The Crystal Structures of TrkA and TrkB Suggest Key Regions for Achieving Selective Inhibition. *J. Mol. Biol.* 2012;423:439–453.

(13) In Vitro Metabolism and Transporter-Mediated Drug-Drug Interaction Studies Guidance for Industry DRAFT GUIDANCE (U.S. Department of Health and Human Services Food and Drug Administration Center for Drug Evaluation and Research (CDER) October 2017 Clinical Pharmacology)

(14) (a) Tao Wang, Michelle L. Lamb, Michael H. Block, *et al*. Discovery of Disubstituted Imidazo[4,5‐b]pyridines and Purines as Potent TrkA Inhibitors. *ACS Med. Chem. Lett.* 2012;13:705−709. (b) Tao Wang, Michelle L. Lamb, David A. Scott, *et al*. Identification of 4-Aminopyrazolylpyrimidines as Potent Inhibitors of Trk Kinases. *J. Med. Chem.* 2008;51:4672-4684.

(15) Maria Menichincheri, Elena Ardini, Paola Magnaghi, et al. Discovery of Entrectinib: A New 3‐Aminoindazole As a Potent Anaplastic Lymphoma Kinase (ALK), c‐ros Oncogene 1 Kinase (ROS1), and Pan-Tropomyosin Receptor Kinases (Pan-TRKs) inhibitor. *J. Med. Chem.* 2016;59:3392−3408

(16) Sarah E. Skerratt, Mark Andrews, Sharan K. Bagal, *et al*. The Discovery of a Potent, Selective, and Peripherally Restricted Pan-Trk Inhibitor (PF-06273340) for the Treatment of Pain. *J. Med. Chem*. 2016;59:10084−10099.

(17) Maria Menichincheri, Elena Ardini, Paola Magnaghi, *et al*. Discovery of Entrectinib: A New 3‐Aminoindazole As a Potent Anaplastic Lymphoma Kinase (ALK), c‐ros Oncogene 1 Kinase (ROS1), and Pan-Tropomyosin Receptor Kinases (Pan-TRKs) inhibitor. *J. Med. Chem.* 2016;59:3392−3408.

(18) Evans DF, Pye G, Bramley R, *et al*. Measurement of gastrointestinal pH profiles in normal ambulant human subjects. Gut. 1988;29:1035−1041.

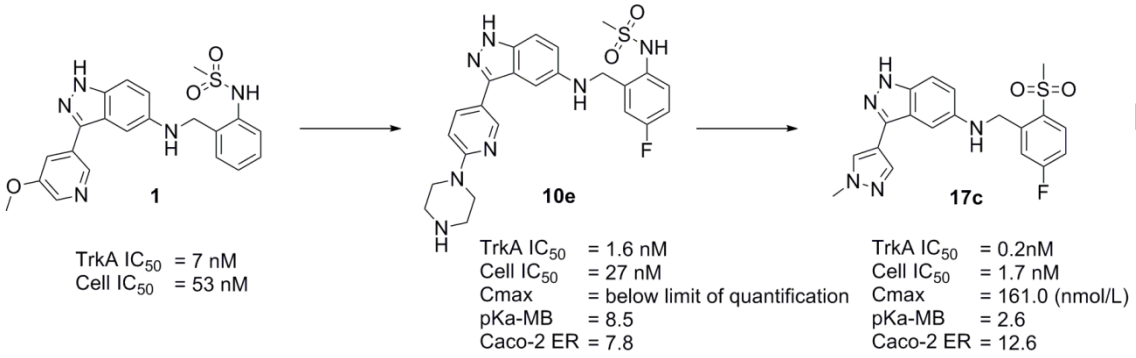

Highlights:

- New 3-Aryl-indazole derivatives as pan-Trk inhibitors were designed and synthesized.
- Substrates for efflux transporter were explored by the Caco-2 assay.
- Membrane permeability was increased by lowing basicity.
- **17c** demonstrated restricted brain penetration and good in vivo efficacy in a CFA-induced thermal hypersensitivity model.